Well-defined insulating band for electronic transport through a laterally coupled double-quantum-dot chain: Nonequilibrium Green's function calculations

Weijiang Gong, Yisong Zheng,* Yu Liu, and Tianquan Lü
Department of Physics, Jilin University, Changchun 130023, China
(Received 18 January 2006; revised manuscript received 7 April 2006; published 23 June 2006)

By means of the nonequilibrium Green function technique, electronic transport through a multiple-quantum-dot system is theoretically studied. In this system, a one-dimensional quantum dot chain between two contacts forms a main channel for the electronic tunneling. Each quantum dot in the chain couples laterally to a dangling quantum dot. Whenever the energy of the incident electron is aligned with the energy levels of the dangling quantum dots, a zero point of the electron transmission function occurs due to the Fano antiresonance. As a result, the linear conductance spectrum presents an insulating band around the antiresonant point. What is interesting is that both edges of the insulating band become steep rapidly with the increase in the numbers of quantum dots. The many-body effect due to the intradot electron interaction on the profile of the insulating band is also investigated by using the equation-of-motion method of the Green functions up to the second-order approximation. It is found that the well-defined insulating band remains. On the basis of this feature, we propose that such a double-quantum-dot chain can be considered as a device prototype of a spin filter.

DOI: 10.1103/PhysRevB.73.245329 PACS number(s): 73.63.Kv, 73.21.La, 73.23.Ra, 73.63.Nm

I. INTRODUCTION

It is well known that most electronic transport properties in the mesoscopic systems are dominated by the quantum coherence phenomenon. The quantum dot (QD) is a typical mesoscopic structure characterized by the discrete electron energy spectrum and the strong electron interaction. The discrete energy levels are essential to form the electron resonant tunneling,[1,2] and the electron interaction has a subtle influence on the electron phase coherence.[3] Therefore, the electronic transport structures involving QDs are often employed to study the quantum coherence phenomenon systemically.[4]

In comparison with a single QD structure, electronic transport through mutually coupled multi-QD systems exhibits more intricate behaviors, because these systems provide much more Feynman paths for the electron transmission. Quantum interference of electron waves passing through different Feynman paths brings about abundant transport properties if the size of the multi-QD system is shorter than or comparable to the electron phase coherence length. In addition, the multi-QD systems possess more tunable parameters than a single QD to manipulate the electronic transport behavior. Accordingly, many schemes of device application are proposed on the basis of electronic transport properties through multi-QD systems, such as quantum computation[5,6] and quantum logic gate.[7]

Recently, many experimental and theoretical works have become increasingly concerned about the electronic transport through various multi-QD systems. For example, in the structures with one or several quantum dots side-coupled to a main conducting channel, some theoretical works showed that a zero point of the linear conductance occurs when the electron Fermi level coincides with the eigenenergy of the dangling QDs.[8–19] The occurrence of a zero point of the linear conductance is interpreted as the destructive quantum interference among electron waves going through different paths. Therefore, it is actually ascribed to the Fano effect. It is called antiresonance in the literature, in contrast with resonance, which gives the conductance peaks. Quite recently, a theoretical prediction about antiresonance was observed experimentally,[12,13] which stimulated further theoretical interest in this topic.[14–19] In particular, some possible device applications based on antiresonance in various coupled QD structures were proposed.[18,19]

In the present work, we will focus on electronic transport through a laterally coupled double-QD chain. The characteristic of such a structure is that some QDs connect in series to form a main chain for the electron tunneling. To each QD in the main chain, there is a side QD attached. We regard a QD in the main chain and the side QD attached to it as a double-QD molecule, which is the basic cell constituting the total structure. It is known from previous works that only one such basic cell can essentially lead to the occurrence of antiresonance (the so-called T-shaped connection of a double-QD with two contacts).[12,13,18] The antiresonant point just coincides with the energy level of the dangling QD. Therefore, we will call such a double-QD molecule an antiresonance cell (ARC) hereafter. The laterally coupled double-QD chain that we will address consists of multiple ARCs. Our purpose is to study the role of antiresonance on electronic transport when the electron tunnels through multiple ARCs coherently. We will see that this structure is not a trivial extension of a one-ARC structure. Instead, a well-defined insulating band forms around the antiresonant point with an increase of the ARCs.

The rest of the paper is organized as follows. In Sec. II, the model Hamiltonian to describe electron behavior in the double-QD chain is introduced first. Then a formula for linear conductance is derived by means of the nonequilibrium Green function technique. In Sec. III, the calculated results regarding the conductance spectrum are shown. Then a discussion on the numerical results, particularly those concerning the formation of the insulating band, is given. Finally, the main results are summarized in Sec. IV.

 ©2006 The American Physical Society

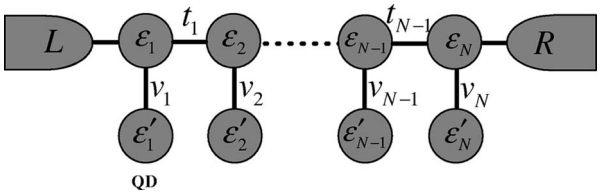

FIG. 1. A schematic illustration of the laterally coupled double-QD chain with length N. The left and right contacts coupled to the double-QD chain in series serve as two electron reservoirs. Each QD in the main chain and the side QD attached to it can be regarded as an antiresonance cell.

II. THE THEORETICAL MODEL

The structure of the laterally coupled double-QD chain we consider is schematically illustrated in Fig. 1. The electron motion in this system can be well described by a generalized Anderson impurity Hamiltonian that reads

$$H = H_C + H_D + H_T + H_{e\text{-}e}, \tag{1}$$

where H_C and H_D are the Hamiltonians in two contacts and the QDs, respectively, H_T describes the electron tunneling between the contacts and the QDs, and $H_{e\text{-}e}$ denotes the many-body term due to the electron interaction. They are given by

$$H_C = \sum_{k\sigma\alpha\in L,R} \varepsilon_{k\alpha} c^{\dagger}_{k\alpha\sigma} c_{k\alpha\sigma},$$

$$H_D = \sum_{\sigma,j=1}^{N} \varepsilon_j d^{\dagger}_{j\sigma} d_{j\sigma} + \sum_{\sigma,j=1}^{N} \varepsilon'_j a^{\dagger}_{j\sigma} a_{j\sigma} + \sum_{\sigma,j=1}^{N-1} (t_j d^{\dagger}_{j+1\sigma} d_{j\sigma} + \text{H.c.}) + \sum_{\sigma,j=1}^{N} (v_j d^{\dagger}_{j\sigma} a_{j\sigma} + \text{H.c.}),$$

$$H_T = \sum_{k\sigma} (V_L c^{\dagger}_{kL\sigma} d_{1\sigma} + \text{H.c.}) + \sum_{k\sigma} (V_R c^{\dagger}_{kR\sigma} d_{N\sigma} + \text{H.c.}),$$

$$H_{e\text{-}e} = \sum_{j=1}^{N} U_j n_{j\uparrow} n_{j\downarrow} + \sum_{j=1}^{N} U'_j n'_{j\uparrow} n'_{j\downarrow}. \tag{2}$$

In the above equations, $c^{\dagger}_{k\alpha\sigma}$, $d^{\dagger}_{j\sigma}$, and $a^{\dagger}_{j\sigma}$ ($c_{k\alpha\sigma}$, $d_{j\sigma}$, and $a_{j\sigma}$) are operators to create (annihilate) an electron of the continuous state k in the contacts, in the jth QD in the main chain, and the side QD attached to it, respectively. $\alpha=L$ or R represents the two contacts and σ the spin index. $\varepsilon_{k\alpha}$, ε_j, and ε'_j denote the corresponding energy levels. t_j is the interdot coupling coefficient between the jth and the $(j+1)$th QDs in the main chain. v_j is the interdot coupling coefficient between the jth QD in the main chain and the side QD attached to it. V_L and V_R denote the coupling between the QD chain and two contacts, which are simplified as constants (we assume $V_L=V_R=V$ in the following calculation). $n_{j\sigma}=d^{\dagger}_{j\sigma}d_{j\sigma}$ and $n'_{j\sigma}=a^{\dagger}_{j\sigma}a_{j\sigma}$ with $\sigma=\uparrow$ or $\downarrow$ are the electron number operators in the jth QD in the main chain and its attachment. U_j and U'_j indicate the strength of intradot Coulomb repulsion of the electrons in the corresponding QDs. All the interdot electron interactions are ignored since they are usually much smaller than the intradot interactions due to the screening effect.

In steady state, the current can be calculated in terms of time evolution of the occupation number of electrons in either contact, say, the left contact. This leads to an expression about the current as[20,21]

$$J_L = \frac{ie}{h}\sum_{\sigma}\int_{-\infty}^{+\infty} d\omega \Gamma^L \{f_L(\omega)[G^r_{11,\sigma}(\omega) - G^a_{11,\sigma}(\omega)] + G^<_{11,\sigma}(\omega)\}, \tag{3}$$

where $f_L(\omega)=1/[1+\exp(\omega-\mu_L)/k_BT]$ is the Fermi function in the left contact; $\Gamma^L=2\pi|V_L|^2\rho(\omega)$ indicates the coupling strength between the left contact and the first QD in the main chain. We will ignore the ω dependence of Γ^L since the electron density of states in the left contact, $\rho(\omega)$, can be usually viewed as a constant. Similarly, we can define Γ^R, the coupling coefficient associated with the right contact. Because we only consider the symmetric coupling between the contacts and the QDs by the assumption $V_L=V_R=V$, we can let $\Gamma^L=\Gamma^R=\Gamma_0$ hereafter. In Eq. (3), the retarded, advanced, and lesser Green functions in Fourier space are involved. They are defined as follows: $G^r_{jl,\sigma}(t)=-i\theta(t)\langle\{d_{j\sigma}(t),d^{\dagger}_{l\sigma}\}\rangle$, $G^a_{jl,\sigma}(t)=i\theta(-t)\langle\{d_{j\sigma}(t),d^{\dagger}_{l\sigma}\}\rangle$, and $G^<_{jl,\sigma}(t)=i\langle d^{\dagger}_{l\sigma}d_{j\sigma}(t)\rangle$, where $\theta(x)$ is the step function. The Fourier transforms of the Green functions can be performed via $G^{r(a,<)}_{jl,\sigma}(\omega)=\int_{-\infty}^{\infty}G^{r(a,<)}_{jl,\sigma}(t)e^{i\omega t}dt$. These Green functions can be solved by means of the equation-of-motion method. For convenience, we employ an alternative notation $\langle\langle A|B\rangle\rangle^x$ with $x=r,a$ or $<$ to denote the Green functions in Fourier space, e.g., $G^r_{jl,\sigma}(\omega)$ is identical to $\langle\langle d_{j\sigma}|d^{\dagger}_{l\sigma}\rangle\rangle^r$. In general, the Green functions obey the following equations of motion, respectively:

$$(\omega \pm i0^+)\langle\langle A|B\rangle\rangle^{r(a)} = \langle\{A,B\}\rangle + \langle\langle [A,H]|B\rangle\rangle^{r(a)}, \tag{4}$$

$$\omega\langle\langle A|B\rangle\rangle^{<} = \langle\langle [A,H]|B\rangle\rangle^{<}. \tag{5}$$

Starting from Eq. (4), we can first derive the equation of motion of the retarded Green function $\langle\langle d_{j\sigma}|d^{\dagger}_{l\sigma}\rangle\rangle^r$ between two arbitrary QDs in the main chain, which yields

$$\left(z-\varepsilon_j+i\frac{\Gamma_0}{2}\delta_{j1}+i\frac{\Gamma_0}{2}\delta_{jN}\right)\langle\langle d_{j\sigma}|d^{\dagger}_{l\sigma}\rangle\rangle^r = \delta_{jl} + t_{j-1}(1-\delta_{j1})\langle\langle d_{j-1\sigma}|d^{\dagger}_{l\sigma}\rangle\rangle^r + t^*_j(1-\delta_{jN})\langle\langle d_{j+1\sigma}|d^{\dagger}_{l\sigma}\rangle\rangle^r + v_j\langle\langle a_{j\sigma}|d^{\dagger}_{l\sigma}\rangle\rangle^r + U_j\langle\langle d_{j\sigma}n_{j\bar{\sigma}}|d^{\dagger}_{l\sigma}\rangle\rangle^r, \tag{6}$$

where the notation $z=\omega+i0^+$ is used. In the above equation, besides the Green functions $\langle\langle d_{j\sigma}|d^{\dagger}_{l\sigma}\rangle\rangle^r$ and $\langle\langle d_{j\pm1\sigma}|d^{\dagger}_{l\sigma}\rangle\rangle^r$ with which we are concerned, two new Green functions are inevitably involved. They are $\langle\langle a_{j\sigma}|d^{\dagger}_{l\sigma}\rangle\rangle^r$ and $\langle\langle d_{j\sigma}n_{j\bar{\sigma}}|d^{\dagger}_{l\sigma}\rangle\rangle^r$. We thus need to work out their equations of motion further. However, because of the many-body terms in the Hamiltonian, we have to truncate the equations of motion at some order to form a closed set of equations. The roughest approach is the Hartree-Fock approximation, which means that $\langle\langle d_{j\sigma}n_{j\bar{\sigma}}|d^{\dagger}_{l\sigma}\rangle\rangle^r \approx \langle n_{j\bar{\sigma}}\rangle\langle\langle d_{j\sigma}|d^{\dagger}_{l\sigma}\rangle\rangle^r$ and $\langle\langle a_{j\sigma}n'_{j\bar{\sigma}}|d^{\dagger}_{l\sigma}\rangle\rangle^r \approx \langle n'_{j\bar{\sigma}}\rangle\langle\langle a_{j\sigma}|d^{\dagger}_{l\sigma}\rangle\rangle^r$ are adopted to deal with

these Green functions associated with the many-body terms. Beyond the Hartree-Fock approximation, we arrive at the second-order approximation, which is to truncate the equations of motion of the Green functions $\langle\langle a_{j\sigma}|d^{\dagger}_{l\sigma}\rangle\rangle^r$, $\langle\langle a_{j\sigma}n'_{j\bar{\sigma}}|d^{\dagger}_{j\sigma}\rangle\rangle^r$, and $\langle\langle d_{j\sigma}n_{j\bar{\sigma}}|d^{\dagger}_{l\sigma}\rangle\rangle^r$ in the following way:

$$(z-\varepsilon'_j)\langle\langle a_{j\sigma}|d^{\dagger}_{j\sigma}\rangle\rangle^r = v^*_j\langle\langle d_{j\sigma}|d^{\dagger}_{j\sigma}\rangle\rangle^r + U'_j\langle\langle a_{j\sigma}n'_{j\bar{\sigma}}|d^{\dagger}_{j\sigma}\rangle\rangle^r, \tag{7}$$

$$(z-\varepsilon'_j-U'_j)\langle\langle a_{j\sigma}n'_{j\bar{\sigma}}|d^{\dagger}_{j\sigma}\rangle\rangle^r = v^*_j\langle n'_{j\bar{\sigma}}\rangle\langle\langle d_{j\sigma}|d^{\dagger}_{j\sigma}\rangle\rangle^r, \tag{8}$$

$$\begin{aligned}(z-\varepsilon_j-U_j)&\langle\langle d_{j\sigma}n_{j\bar{\sigma}}|d^{\dagger}_{l\sigma}\rangle\rangle^r \\ &= \langle n_{j\bar{\sigma}}\rangle\delta_{jl} + t_{j-1}(1-\delta_{j1})\langle n_{j\bar{\sigma}}\rangle\langle\langle d_{j-1\sigma}|d^{\dagger}_{l\sigma}\rangle\rangle^r \\ &+ t^*_j(1-\delta_{jN})\langle n_{j\bar{\sigma}}\rangle\langle\langle d_{j+1\sigma}|d^{\dagger}_{l\sigma}\rangle\rangle^r + v_j\langle n_{j\bar{\sigma}}\rangle\langle\langle a_{j\sigma}|d^{\dagger}_{l\sigma}\rangle\rangle^r \\ &- \left(i\frac{\Gamma_0}{2}\delta_{j1} + i\frac{\Gamma_0}{2}\delta_{jN}\right)\langle n_{j\bar{\sigma}}\rangle\langle\langle d_{j\sigma}|d^{\dagger}_{l\sigma}\rangle\rangle^r.\end{aligned} \tag{9}$$

In Eqs. (7)–(9), the approximations $\langle\langle d_{j\pm1\sigma}n_{j\bar{\sigma}}|d^{\dagger}_{l\sigma}\rangle\rangle^r \approx \langle n_{j\bar{\sigma}}\rangle\langle\langle d_{j\pm1\sigma}|d^{\dagger}_{l\sigma}\rangle\rangle^r$, $\langle\langle d_{j\sigma}n'_{j\bar{\sigma}}|d^{\dagger}_{j\sigma}\rangle\rangle^r \approx \langle n'_{j\bar{\sigma}}\rangle\langle\langle d_{j\sigma}|d^{\dagger}_{j\sigma}\rangle\rangle^r$ and $\langle\langle c_{k\alpha\sigma}n_{j\bar{\sigma}}|d^{\dagger}_{l\sigma}\rangle\rangle^r \approx \langle n_{j\bar{\sigma}}\rangle\langle\langle c_{k\alpha\sigma}|d^{\dagger}_{l\sigma}\rangle\rangle^r$ have been used to eliminate these high-order Green functions. The cost of such an approach is that the influence of electron correlation on the transport properties is left out, such as the Kondo effect.[22] But the advantage of this approach is that it allows for an explicit expression about the linear conductance in terms of the equilibrium state Green functions, which will be seen below.

The equations of motion of the Green function $G^<_{jl,\sigma}(\omega)$ can be derived in a similar way. But it should be noted that the following relations are used when the two contacts are involved in the equations of motion of the Green functions, i.e.,

$$\begin{aligned}\langle\langle c_{kL\sigma}|d^{\dagger}_{l\sigma}\rangle\rangle^< &= Vg^r_{kL\sigma}(\omega)\langle\langle d_{1\sigma}|d^{\dagger}_{l\sigma}\rangle\rangle^< + Vg^<_{kL\sigma}(\omega)\langle\langle d_{1\sigma}|d^{\dagger}_{l\sigma}\rangle\rangle^a, \\ \langle\langle c_{kR\sigma}|d^{\dagger}_{l\sigma}\rangle\rangle^< &= Vg^r_{kR\sigma}(\omega)\langle\langle d_{N\sigma}|d^{\dagger}_{l\sigma}\rangle\rangle^< + Vg^<_{kR\sigma}(\omega)\langle\langle d_{N\sigma}|d^{\dagger}_{l\sigma}\rangle\rangle^a,\end{aligned} \tag{10}$$

where $g^r_{k\alpha\sigma}(\omega)$ and $g^<_{k\alpha\sigma}(\omega)$ are the free-electron Green functions in the isolated contacts. They take forms as $g^r_{k\alpha\sigma}(\omega) = (\omega-\varepsilon_{k\alpha}+i\eta)^{-1}$ and $g^<_{k\alpha\sigma}(\omega) = 2\pi i f_\alpha \delta(\omega-\varepsilon_{k\alpha})$.

After some derivation, we can obtain the iterative equations about the Green functions $G^r_{jl,\sigma}(\omega)$ and $G^<_{jl,\sigma}(\omega)$, which are crucial for the derivation of the expression about the linear conductance. They are

$$G^r_{jl,\sigma} = \delta_{jl}g_{j\sigma} + t_{j-1}(1-\delta_{j1})g_{j\sigma}G^r_{j-1l,\sigma} + t^*_j(1-\delta_{jN})g_{j\sigma}G^r_{j+1l,\sigma}, \tag{11}$$

$$G^<_{jl,\sigma} = \Delta_{jl}g_{j\sigma} + t_{j-1}(1-\delta_{j1})g_{j\sigma}G^<_{j-1l,\sigma} + t^*_j(1-\delta_{jN})g_{j\sigma}G^<_{j+1l,\sigma}. \tag{12}$$

We can see that the two equations resemble each other except that the Kronecker delta function δ_{jl} in Eq. (11) is replaced by Δ_{jl} in Eq. (12), which is defined by

$$\Delta_{jl} = i\Gamma_0 f_L G^a_{jl,\sigma}\delta_{j1} + i\Gamma_0 f_R G^a_{jl,\sigma}\delta_{jN}. \tag{13}$$

In addition, $g_{j\sigma}$, the Green function of the jth isolated double-QD molecule, has been involved in Eqs. (11) and (12). It takes the form

$$g_{j\sigma} = \frac{S_j(z)}{z-\varepsilon_j + \frac{i\Gamma_0}{2}S_j(z)\delta_{j1} + \frac{i\Gamma_0}{2}S_j(z)\delta_{jN} - \frac{|v_j|^2}{z-\varepsilon'_j}S_j(z)S'_j(z)}, \tag{14}$$

with $S_j(z) = 1+\frac{U_j\langle n_{j\bar{\sigma}}\rangle}{z-\varepsilon_j-U_j}$ and $S'_j(z) = 1+\frac{U'_j\langle n'_{j\bar{\sigma}}\rangle}{z-\varepsilon'_j-U'_j}$, where the average electron occupation numbers in QDs are determined by the relations $\langle n_{j\sigma}\rangle = -\frac{i}{2\pi}\int d\omega\langle\langle d_{j\sigma}|d^{\dagger}_{j\sigma}\rangle\rangle^<$, $\langle n'_{j\sigma}\rangle = -\frac{i}{2\pi}\int d\omega\langle\langle a_{j\sigma}|a^{\dagger}_{j\sigma}\rangle\rangle^<$. As we have done in Eqs. (11)–(14), we will often drop the ω dependence of the Green functions hereafter, in order to make the formulas compact.

We need to point out that when the electron interaction is absent, the set of equations of motion about the retarded and lesser Green functions become exactly closed, and the iterative relations (11) and (12) still hold. But Eq. (14) is reduced as

$$g_{j\sigma} = \frac{1}{z-\varepsilon_j + \frac{i\Gamma_0}{2}\delta_{j1} + \frac{i\Gamma_0}{2}\delta_{jN} - \frac{|v_j|^2}{z-\varepsilon'_j}}. \tag{15}$$

Moreover, in the Hartree-Fock approximation, $g_{j\sigma}$ has the same form as Eq. (15) except that ε_j and ε'_j should be changed to $\varepsilon_j+U_j\langle n_{j\bar{\sigma}}\rangle$ and $\varepsilon'_j+U'_j\langle n'_{j\bar{\sigma}}\rangle$, respectively.

We are now ready to simplify the current formula (3). By defining a tridiagonal matrix D_1 as $[D_1]_{jl} = -t_{j-1}\delta_{lj-1} + g^{-1}_{j\sigma} - t^*_j\delta_{lj+1}$, we infer from Eq. (11) that the retarded Green function in a matrix form can be formally written as $G^r = [D_1]^{-1}$. Prior to further derivation, it is necessary for us to introduce the notation D_i to denote a lower-right-corner submatrix of D_1. The matrix elements of D_i range from ith row (column) to the last row (column) elements of D_1. We thus have $G^r_{11,\sigma} = \det D_2/\det D_1$. Furthermore, we can derive the following relation:

$$\begin{aligned}G^r_{11,\sigma} - G^a_{11,\sigma} &= \frac{\det D_2}{\det D_1} - \frac{\det D^*_2}{\det D^*_1} \\ &= \frac{\det D_2 \det D^*_1 - \det D^*_2 \det D_1}{|\det D_1|^2} \\ &= \frac{[(g^{-1}_{1\sigma})^* - g^{-1}_{1\sigma}]|\det D_2|^2}{|\det D_1|^2} \\ &\quad + \frac{|t_1|^2(\det D_3 \det D^*_2 - \det D^*_3 \det D_2)}{|\det D_1|^2} \\ &= -i\Gamma_0|G^r_{11,\sigma}|^2 - i\Gamma_0|G^r_{1N,\sigma}|^2.\end{aligned} \tag{16}$$

To reach the last step in the above equation, use has been made of the iterative relation $\det D_j = g^{-1}_{j\sigma}\det D_{j+1} - |t_j|^2 \det D_{j+2}$, which is a straightforward result of a tridiagonal matrix.

We now address the lesser Green function. At first we note that Eq. (12) can be abbreviated to $D_1 G^< = \Delta$ where the matrix element of Δ is defined by Eq. (13). Then it can be readily seen that the lesser Green function is just the product of the Green function G^r and the matrix Δ, i.e., $G^< = G^r \Delta$, from which we obtain

$$G^<_{11,\sigma} = i\Gamma_0 f_L |G^r_{11,\sigma}|^2 + i\Gamma_0 f_R |G^r_{1N,\sigma}|^2. \tag{17}$$

Substituting Eqs. (16) and (17) into Eq. (3), we obtain a compact form of the current formula. That is,

$$J_L = \frac{e}{h} \sum_\sigma \int_{-\infty}^{+\infty} d\omega T_\sigma(\omega)[f_L(\omega) - f_R(\omega)], \tag{18}$$

from which the linear conductance can be extracted. It is denoted as

$$\mathcal{G} = \frac{e^2}{h} \sum_\sigma T_\sigma(\omega)\big|_{\omega=\varepsilon_F}, \tag{19}$$

with the transmission function

$$T_\sigma(\omega) = |G^r_{1N,\sigma}(\omega)|^2 \Gamma_0^2. \tag{20}$$

In Eq. (20), the Green function $G^r_{1N,\sigma}$ can be calculated with the help of the iterative relation (11). After some derivation, we obtain an analytical expression about it as

$$G^r_{1N,\sigma}(\omega) = \tau^\sigma_{12} \tau^\sigma_{23} \cdots \tau^\sigma_{N-1N} g_{N\sigma}, \tag{21}$$

where τ^σ_{jj+1} indicates the renormalized interdot transmission coefficient for electrons with spin σ. It is defined as

$$\tau^\sigma_{jj+1} = \frac{g_{j\sigma} t_j}{1 - \dfrac{|t_j|^2}{t_{j+1}} g_{j\sigma} \tau^\sigma_{j+1j+2}} \quad \text{for} \quad 1 \leqslant j < N-1, \tag{22}$$

and the last one is given by

$$\tau^\sigma_{N-1N} = \frac{g_{N-1\sigma} t_{N-1}}{1 - |t_{N-1}|^2 g_{N-1\sigma} g_{N\sigma}}. \tag{23}$$

Substituting the expression of the Green function $G^r_{1N,\sigma}$ into Eq. (20), we arrive at

$$T_\sigma(\omega) = T_{1\sigma}(\omega) T_{2\sigma}(\omega) \cdots T_{N-1\sigma}(\omega) T_{N\sigma}(\omega), \tag{24}$$

by which the transmission function is expressed as a product of the individual transmission functions corresponding to the electron tunneling through each ARC. They are defined as $T_{j\sigma}(\omega) = |\tau^\sigma_{jj+1}|^2$ for $j=1$ to $N-1$ and $T_{N\sigma} = |\Gamma_0 g_{N\sigma}|^2$.

III. NUMERICAL RESULTS AND DISCUSSION

With the solution of the Green function developed in the previous section, we can investigate the linear conductance spectrum of the laterally coupled double-QD chain. To do this, we need to calculate the linear conductance as a function of the QD level, which can be experimentally adjusted by a gate voltage. Before we proceed, we need to introduce a parameter t_0 as the unit of energy. In addition, we can assume that the system has a uniform Fermi energy and take it as the zero point of energy, since the linear conductance is only related to the equilibrium state properties of the system, though the nonequilibrium Green function technique has been used to derive the expression about it.

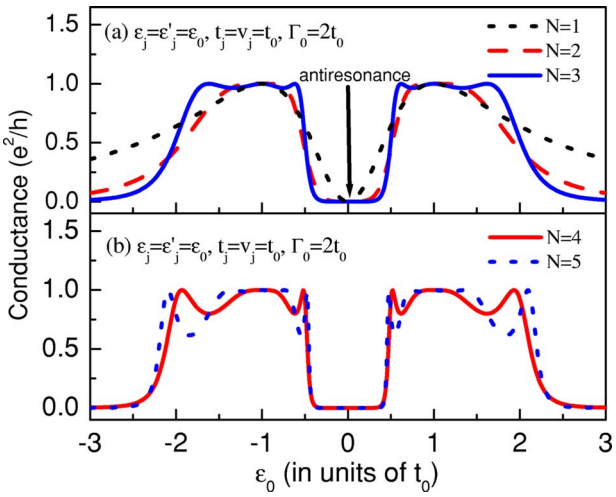

FIG. 2. (Color online) The linear conductance spectra of several laterally coupled double-QD chains. The structure parameters take the following values: $t_j = v_j = t_0$ and $\varepsilon_j = \varepsilon'_j = \varepsilon_0$ for all QDs, where t_0 is the unit of energy; in addition, $\Gamma_0 = 2t_0$, which implies a relatively strong coupling. (a) The linear conductance spectra for the cases of $N=1$ to 3. (b) The linear conductance spectra for the cases of $N=4$ and 5.

First of all, we focus on the characteristics of the linear conductance spectrum in the absence of electron interactions, since we are mainly interested in the antiresonance effect. It has been demonstrated in previous works that the basic aspects of antiresonance can be well elucidated in the single electron picture. We thus leave the many-body effect out by assuming $U_j = U'_j = 0$ for all QDs. As a typical case, we consider a system to have uniform parameters. For instance, we choose the parameter values $v_j = t_j = t_0$ and $\varepsilon_j = \varepsilon'_j = \varepsilon_0$ for all QDs to perform the numerical calculation. It should be noted that the uniform QD level, ε_0, shifts with respect to the Fermi level by adjusting the gate voltage. Besides, we take $\Gamma_0 = 2t_0$ which implies a relatively strong coupling. Figure 2 shows the linear conductance spectra ($\mathcal{G}$ versus ε_0) for several structures with the number of ARC $N=1$ to 5. From this figure we can see that the antiresonance (the zero point of the linear conductance) occurs at $\varepsilon_0 = 0$ for all the structures, regardless of the variation of the length of the double-QD chain. A more interesting result shown in Fig. 2 is that a well-defined insulating band forms around the antiresonant point when $N \geqslant 3$. In Fig. 2(a), we can see that both edges of the antiresonance valley become steep rapidly while N increases from 1 to 3. The results shown in Fig. 2(b) indicate that when $N > 3$, the antiresonance valley has changed into a well-defined insulating band, the shape of which is almost fixed even if N increases further.

The occurrence of the well-defined insulating band is tightly associated with the antiresonance phenomenon. In Fig. 3, the calculated results about the individual transmission functions are shown for a five-ARC structure (namely, a laterally coupled double-QD chain with $N=5$). We can find

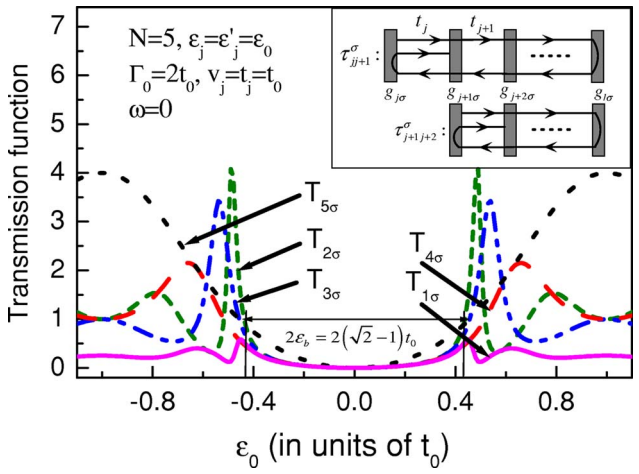

FIG. 3. (Color online) The individual transmission function of a laterally coupled double-QD chain with $N=5$ as a function of the QD energy level. The parameters take the same values as the case shown in Fig. 2(b). Besides, $\omega=\varepsilon_F=0$ is set. The quantity $2E_b=2(\sqrt{2}-1)t_0$ labels the width of the insulating band. The inset shows two typical Feynman paths belonging to τ^{σ}_{jj+1} and τ^{σ}_{j+1j+2}, respectively.

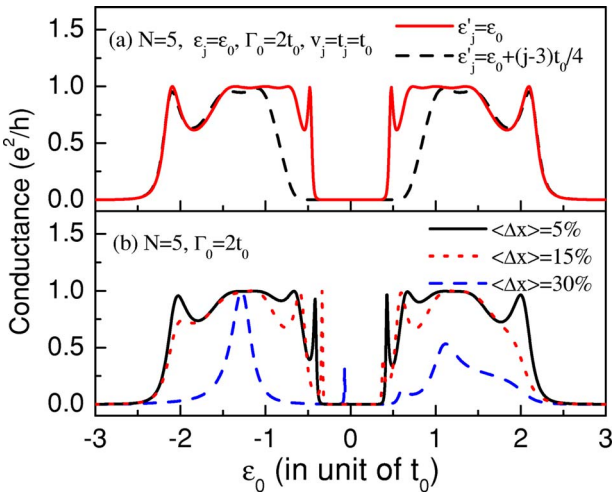

FIG. 4. (Color online) (a) A comparison of conductance spectra between two different five-ARC structures. Solid line: a replot of the conductance spectrum for the $N=5$ structure shown in Fig. 2(b). Dashed line: the energy levels of the side QDs are given by $\varepsilon'_j=\varepsilon_0+(j-3)t_0/4$. The other parameters take the same values as the case shown by the solid line. In this case, the insulating band broadens but both edges are not very sharp. (b) The conductance spectra of the five-ARC structures with fluctuated QD parameters. The fluctuation is measured by the standard deviation $\langle\Delta x\rangle=[\Sigma_j x_j^2/N-(\Sigma_j x_j/N)^2]^{1/2}/t_0$ with $x_j=\varepsilon_j$, ε'_j, t_i, and v_j. The solid line denotes the case of $\langle\Delta x\rangle=5\%$, in which the well-defined insulating band remains. The dotted line for $\langle\Delta x\rangle=15\%$ and the dashed line for $\langle\Delta x\rangle=30\%$. These results indicate that the increment of fluctuation can destroy the well-defined insulating band.

that two common features of the individual transmission functions are crucial for the formation of the well-defined insulating band. First, each transmission function exhibits antiresonance at $\varepsilon_0=0$, since they all include $g_{j\sigma}$'s as factors, see Eqs. (22) and (23). Secondly, their profiles resemble each other in the antiresonance valley ($T_{1\sigma}$ and $T_{N\sigma}$ show trivial deviations from the others because of the effect of the two contacts). This can be explained in the language of Feynman paths.[23] To expand Eq. (22), the expression of the transmission coefficient, as an infinite geometric series, we realize that each τ^{σ}_{jj+1} can be regarded as the sum of the contributions of infinitely multiple Feynman paths. In such a viewpoint, we can express the transmission coefficient as

$$\tau^{\sigma}_{jj+1}=\sum_p A_p(j,j+1),$$

$$P \in \text{ all paths starting at } j \text{ and ending at } j+1. \tag{25}$$

A typical path may be expressed as

$$A_p(j,j+1)=g_{j\sigma}t_j g_{j+1\sigma}t_{j+1}g_{j+2\sigma}\cdots g_{l\sigma}t_{l-1}g_{l-1\sigma}\cdots t_j g_{j\sigma}t_j. \tag{26}$$

Obviously, τ^{σ}_{jj+1} possesses longer Feynman paths than τ^{σ}_{j+1j+2} since every path belonging to the latter can be included as a part of a path belonging to the former. This is illustrated by the inset of Fig. 3. However, in the antiresonance valley the long Feynman paths do not contribute much to τ^{σ}_{jj+1} since the factors $g_{j\sigma}$ guarantee the series converges rapidly. Consequently, τ^{σ}_{jj+1} does not deviate from τ^{σ}_{j+1j+2} nontrivially in the antiresonance valley, hence the resemblance to the individual transmission functions in this region. Therefore, we can approximate the total transmission function in the antiresonance valley as $T_\sigma(\omega)\approx[T_{j\sigma}(\omega)]^N$. On the basis of this argument, it is not difficult to understand the formation of a well-defined insulating band. The band edge occurs at ε_b satisfying $T_{j\sigma}(\varepsilon_b)=1$. We can determine the band edge in the following way. In Eq. (22), we let $\tau^{\sigma}_{jj+1}=\tau^{\sigma}_{j+1j+2}=\tau^{*}_{\sigma}(\varepsilon)$. Then we can solve the steady transmission coefficient $\tau^{*}_{\sigma}(\varepsilon)$, which yields

$$\tau^{*}_{\sigma}(\varepsilon)=\frac{g^{-1}_{j\sigma}\pm\sqrt{g^{-2}_{j\sigma}-4t_0^2}}{2t_0}. \tag{27}$$

By the condition $|\tau^{*}_{\sigma}(\varepsilon_b)|=1$, we obtain the band edge to occur at $\pm\varepsilon_b$, with $\varepsilon_b=(\sqrt{2}-1)t_0$, which is just the edges of the energy bands of the infinite double-QD chain.

In Fig. 4(a), the linear conductance spectrum is shown for another five-ARC structure, in which the parameter values are taken as $\varepsilon_j=\varepsilon_0$ and $\varepsilon'_j=\varepsilon_0+(j-3)t_0/4$. We can see that the insulating band broadens notably. However, both edges of it are not as sharp as the previous one, where all the QD levels take a uniform value. Such a difference can be readily understood according to the argument stated above. The band broadening arises from the fact that the antiresonant points of the individual ARCs are no longer located at the same point. Instead, they are distributed in a relatively wide region. On the other hand, the different locations of the antiresonant points cause the antiresonance valleys of the individual transmission functions to deviate from each other, which goes against the formation of a very sharp insulating band.

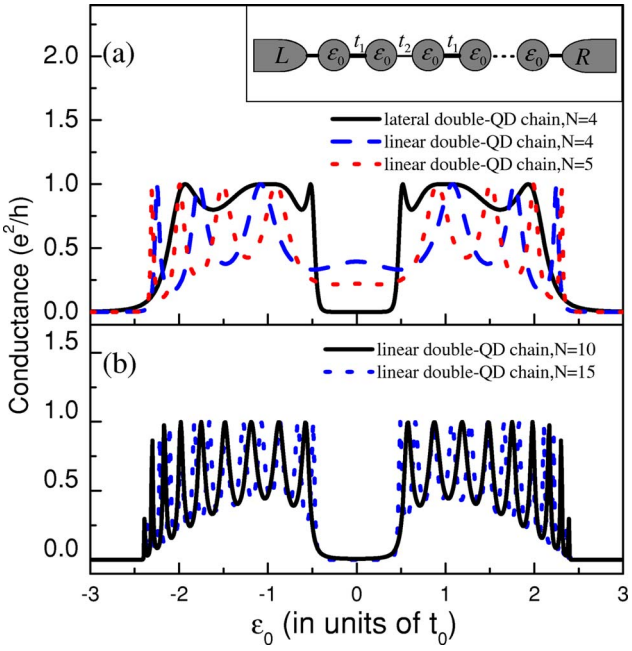

FIG. 5. (Color online) (a) A comparison of the linear conductance spectra between the laterally coupled double-QD chain with $N=4$ and the linear double-QD chain with $N=4$ and 5. The structure of the linear double-QD chain is illustrated by the inset. The parameter values are given as follows: $\Gamma_0=2t_0$. All the QD levels take the uniform value as ε_0. For the lateral chain, we assume $t_j=v_j=t_0$, but for the linear chain we let $t_1=t_0$ and $t_2=\sqrt{2}t_0$ to form a double-QD chain. (b) The linear conductance spectra of the linear double-QD chain for $N=10$ and 15.

This result indicates that the uniformity of the QD chain, especially the identical levels of the dangling QDs, is a crucial condition for the formation of a sharp insulating band. However, so far it is still a formidable challenge to fabricate experimentally an electron transport chain consisting of identical and uniformly coupled QDs, though there have been some reports about the growth of identical QD arrays on a semiconductor surface.[24,25] Therefore, it is necessary to investigate the sensitivity of the sharp insulating band to the uniformity of the QD chain. We calculate the conductance spectrum of a five-ARC structure with fluctuated QD parameters. The result is shown in Fig. 4(b). When the fluctuation is relatively small [$\sim 5\%$ in Fig. 4(b)], the well-defined insulating band remains in the spectrum. But the increment of the fluctuation destroys the well-defined insulating band indeed. The average energy band gap of an infinite chain is a critical quantity to measure the fluctuation (we have mentioned how to get the band gap in the above, but we need to use the average QD parameters to evaluate the average band gap). When the fluctuation is comparable with this gap, the picture of the energy band becomes invalid. Furthermore, the antiresonant points of the individual ARC are distributed randomly in a rather wide range. Thus, the insulating band becomes ill-defined, or fully vanishing. Our conclusion is that the well-defined band does not require an absolute uniformity of the QD chain, but the fluctuation should be far smaller than the average band gap. In addition, we would like to point out that some polymer materials with dangling

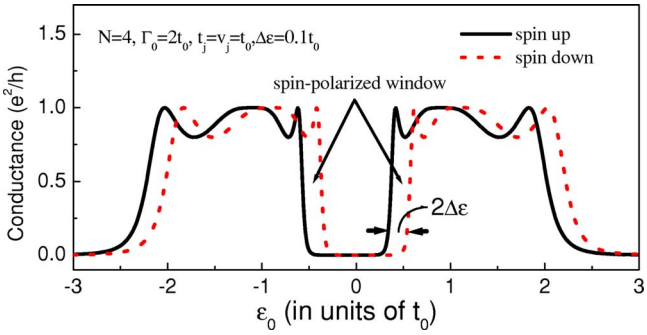

FIG. 6. (Color online) The spin split of the linear conductance spectrum of the laterally coupled double-QD chain. The parameter values are given as follows. $N=4$, $t_j=v_j=t_0$, and $\Gamma_0=2t_0$. The spin-dependent QD levels are $\varepsilon_{j\uparrow}=\varepsilon'_{j\uparrow}=\varepsilon_0+\Delta\varepsilon$ and $\varepsilon_{j\downarrow}=\varepsilon'_{j\downarrow}=\varepsilon_0-\Delta\varepsilon$. The solid line indicates the linear conductance for the spin-up electron and the dotted line for that of the spin-down electron. As pointed by the arrows, two spin-polarized windows emerge.

bonds may be the better candidates than the present QD chain to demonstrate our theoretical prediction, since the uniformity is a natural characteristic of polymers.

To see more clearly the crucial role of antiresonance on the formation of the well-defined insulating band, it is helpful to compare the conductance behaviors between our structure and a linearly coupled double-QD chain. For example, from a QD single chain between two contacts, we can obtain a linear double-QD chain by adopting two different interdot couplings alternately, see the inset in Fig. 5(a). In analogy with our structure, this linear double-QD chain also has two energy bands with a gap in between. However, unlike our structure, no antiresonance happens in this structure. Figure 5 shows a comparison of the calculated linear conductances between the linear double-QD chain and our structure. When the number of ARCs is small, e.g., $N=4$ and 5, the conductance spectrum of the linear double-QD chain does not present a well-defined insulating band, as shown in Fig. 5(a). Once the chain becomes very long, an insulating band emerges, which coincides with the gap between the energy bands of the linear double-QD chain. Such a result is shown in Fig. 5(b). From such a comparison, we can conclude that the antiresonance plays a crucial role in the occurrence of a well-defined insulating band.

Now we consider an interesting case that could be instructive to the device application. In our structure, we assume that the QD levels are spin-dependent, which can be realized by applying a magnetic field on them or assuming them to be made of ferromagnetic material. Then the conductance spectra of the electrons with opposite spins will separate from each other. Because both edges of the insulating band are very steep, it is easy to form a window where the electrons in one spin direction can tunnel through the structure nearly transparently, while the tunneling of the electrons with opposite spins is hardly allowed. To visualize this scheme, we take the following parameter values to evaluate the linear conductance. For all QDs, the spin-dependent energy levels are $\varepsilon_{j\uparrow}=\varepsilon'_{j\uparrow}=\varepsilon_0+\Delta\varepsilon$ and $\varepsilon_{j\downarrow}=\varepsilon'_{j\downarrow}=\varepsilon_0-\Delta\varepsilon$, respectively. Besides, we let $t_j=v_j=t_0$ and $\Gamma_0=2t_0$. The spin split may arise from the Zeeman energy or the exchange energy. Figure 6

shows the calculated results about the conductance spectra of the electrons with both spins. As we expected, two windows emerge, as marked by the arrows in the figure. And the width of the window is just equal to the spin splitting $2\Delta\varepsilon$. Thus, if the electronic transport is set to run in the window region by tuning the gate voltage, we can implement a highly spin-polarized current flow. Therefore, we suggest that such a double-QD structure can be considered to be a device prototype of a spin filter. To the best of our knowledge, there are some similar proposals based on the interplay of resonance and antiresonance between electrons with opposite spins.[10,18,19,26,27] However, our structure is apt to establish a highly spin-polarized window due to the existence of a well-defined insulating band.

Next, we consider the many-body effect on the linear conductance spectrum. Our purpose is to explore whether the electron interaction can destroy the well-defined insulating band strikingly. To calculate the linear conductance, we use the same parameter values as the case shown in Fig. 1. As for the many-body terms, we assume a uniform Coulomb repulsion U for all QDs. First, we deal with this problem in the Hartree-Fock approximation. Thus we have to restrict our calculation in a regime with $U \ll t_0$, since the electron correlation effect becomes significant with the increase of the Coulomb repulsion. In the Hartree-Fock approximation, the Hamiltonian has the same structure as the noninteracting one, except that the QD levels become electron-occupation-dependent, i.e., $\varepsilon_j \rightarrow \varepsilon_{j\sigma} + U\langle n_{j\bar{\sigma}}\rangle$. Therefore, we anticipate that the well-defined insulating band will remain. This is demonstrated by the calculated result shown in Figs. 7(a) and 7(b). We find that the effect of electron interaction in the Hartree-Fock approximation is only to shift the insulating band to the lower direction, without a remarkable modification on the shape of the insulating band. The shift can be easily explained. In the Hartree-Fock approximation, the antiresonance occurs at $\varepsilon'_j + U\langle n'_{j\bar{\sigma}}\rangle = 0$. Because $U\langle n'_{j\bar{\sigma}}\rangle$ is always a positive term, the total insulating band as well as the antiresonant point shifts toward the left. In Fig. 7(c), the spin split of the linear conductance spectrum is shown by assuming a Zeeman energy $\Delta_\varepsilon = 0.1t_0$. We can see that two spin-polarized windows emerge. In contrast with the result shown in Fig. 6, in this case the window width originates from not only the Zeeman energy but also the Coulomb repulsion, i.e., $\Delta_s = 2\Delta\varepsilon + U|\langle n'_{j\downarrow}\rangle - \langle n'_{j\uparrow}\rangle|$. From this result, we can infer that using small QDs in our structure is advantageous to realizing the spin filter since the Coulomb repulsion increases as the sizes of QDs diminish. But a prerequisite is whether a strong Coulomb repulsion can destroy the sharp edges of the insulating band, beyond the Hartree-Fock approximation.

Figure 8(a) shows the calculated conductance spectrum by incorporating the many-body effect to second order. In such a case, we can consider a relatively strong Coulomb repulsion. We can find that the insulating band splits into two bands due to the strong Coulomb repulsion. But the steep edges of the bands survive. In addition, between both separated bands there is a narrow band that arises from the electron-hole symmetry.[28–30] At the specific condition of $\varepsilon_0 = -U/2$, the Hamiltonian possesses electron-hole symmetry, which leads to $\langle n_{j\uparrow}\rangle = \langle n_{j\downarrow}\rangle = 1/2$. From Eq. (14), it can be

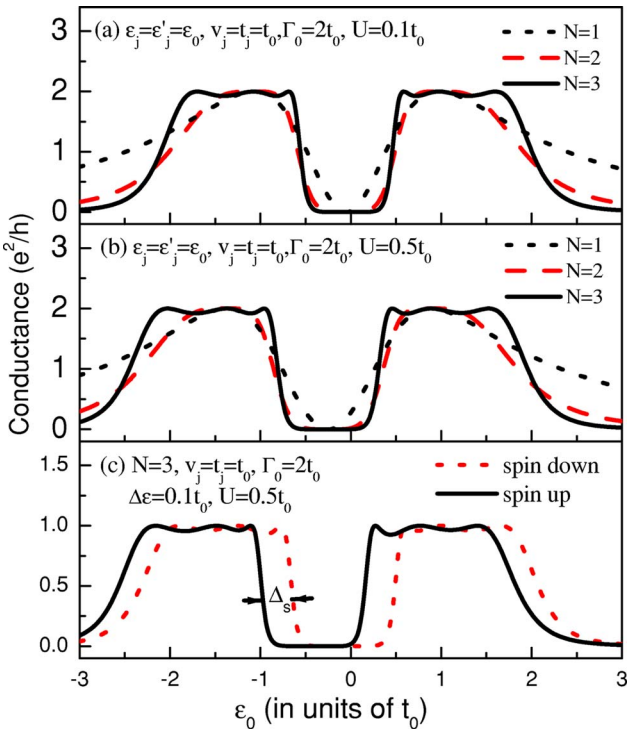

FIG. 7. (Color online) The linear conductance spectra of the laterally coupled double-QD chains with $N=1$, 2, and 3, calculated within the Hartree-Fock approximation. The parameters take the values as $\Gamma_0 = 2t_0$, $\varepsilon_j = \varepsilon'_j = \varepsilon_0$, and $t_j = v_j = t_0$ for all QDs. Besides, a uniform Coulomb repulsion is assumed. (a) The case of $U=0.1t_0$. (b) The case of $U=0.5t_0$. (c) The spin-dependent conductance spectrum for $N=3$ structure with $U=0.5t_0$, but the QD levels have the spin-split $\Delta\varepsilon = 0.1t_0$. Δ_s denotes the width of the spin-polarized window, which broadens due to the contribution of the electron interaction, in comparison with the case shown in Fig. 5. The solid line indicates the linear conductance for the spin-up electron and the dotted line for that of the spin-down electron.

seen that $g_{j\sigma}(0) = 0$ because of the factor $S_j(0) = 0$. Thus, the electron-hole symmetry causes antiresonance, which evolves into an insulating band with the increase of N. However, the antiresonance resulting from the electron-hole symmetry seems to be a pseudo one. In some previous works, it was proved that the electron-hole symmetry does not bring about antiresonance when a higher approximation is used to handle the many-body effect.[22] In Fig. 8(b), the spin split of the conductance spectrum is plotted. Like the result of the Hartree-Fock approximation, we can find that the spin-polarized window broadens by the strong Coulomb repulsion between electrons.

With regard to the many-body effect, we should emphasize the following point. Our calculation indicates that the electron interaction does not destroy the well-defined insulating band strikingly. However, we have taken the many-body terms into account within the approximations only to second order. Therefore, to what extent the well-defined insulating band survives is still in question if the many-body effect is incorporated up to higher orders, especially in the strong correlation regime. For example, it is known for sure that the Kondo resonance must give a modification on the

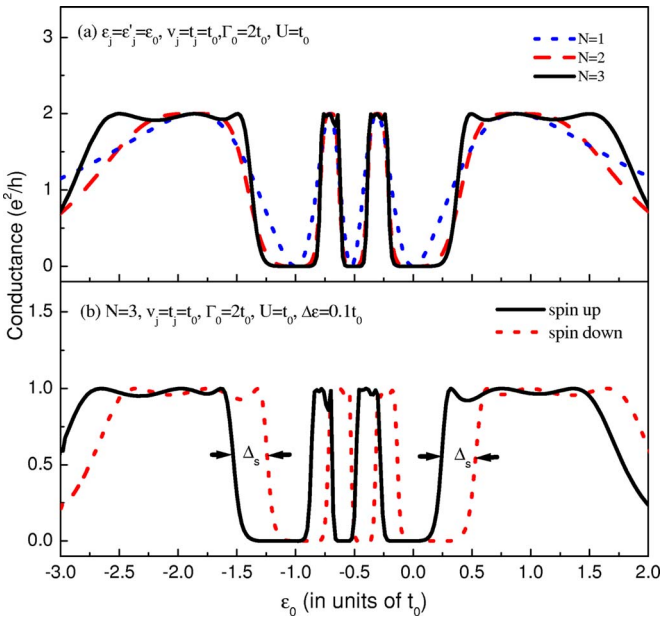

FIG. 8. (Color online) (a) The linear conductance spectra of the laterally coupled double-QD chain with $N=1$, 2, and 3. The many-body effect is incorporated to second order in the calculation. The parameter values are $\Gamma_0=2t_0$, $U=t_0$, $\varepsilon_j=\varepsilon'_j=\varepsilon_0$, and $t_j=v_j=t_0$ for all QDs. (b) The spin split of the linear conductance spectrum of an $N=3$ structure with $\Delta\varepsilon=0.1t_0$. The spin-polarized window broadens due to the many-body effect.

linear conductance spectrum when the QD levels are far below the Fermi energy.[31,32] However, as we have shown, the well-defined insulating band occurs in the mixed-valence regime, not the Kondo regime for the uniform structure. Of course, one can pay attention to the influence of Kondo resonance on the insulating band by setting the QDs in the main chain in the Kondo regime, while the side QDs are in the mixed-valence regime. Such an interesting topic is beyond the scope of the present work, and will be left for future study.

IV. SUMMARY

By means of a generalized Anderson impurity Hamiltonian, we have investigated the electronic transport properties through a laterally coupled double-QD chain. The calculated linear conductance spectrum exhibits a well-defined insulating band. To form such a very steep band does not require a very long chain, though its width coincides with the gap between the bonding and antibonding bands of an infinite double-QD chain. The underlying physics for the formation of the well-defined insulating band is the antiresonance effect arising from the existence of the attached QDs. Each double-QD molecule can be regarded as an antiresonance cell. The electron transmission in the antiresonance valley is further suppressed whenever the electrons pass through one more antiresonance cell. As a result, the insulating band forms rapidly. When $N=4$, which is still a quite short chain, the band edge becomes very steep and almost fixed. Moreover, the influence of the many-body effect on the well-defined insulating band is discussed in the Hartree-Fock and second-order approximations. Our conclusion is that the many-body effect does not influence notably the shape of the insulating band. On the basis of this feature, we suggest a potential device application of such a structure as a spin filter. Because of the existence of the steep band edges, it is very easy to create a highly spin-polarized window when the electrons tunnel through this structure. In addition, selecting smaller QDs is advantageous for the realization of a spin filter, because the stronger electron interaction can enlarge the width of the spin-polarized window. Quite recently, we found that a similar insulating band has been predicted in a quantum waveguide with serial stubs by a different theoretical approach.[33] But in this paper we have presented a reasonable explanation of this feature in terms of antiresonance and we have discussed the influence of the many-body effect. Thereby the physical picture of this issue becomes clear. According to our result, the occurrence of the well-defined insulating band can be generalized to any one-dimensional chain of quantum levels with some dangling bonds.

ACKNOWLEDGMENTS

This work was financially supported by the National Natural Science Foundation of China under Grant No. NNSFC69971012.

*Author to whom correspondence should be addressed. Email address: zys@mail.jlu.edu.cn

[1] L. P. Kouwenhoven, C. M. Marcus, P. L. McEuen, S. Tarucha, R. M. Westervelt, and N. S. Wingreen, in *Mesoscopic Electron Transport*, Proceedings of the NATO Advanced Study Institute on Mesoscopic Electron Transport, Series E345, edited by L. L. Sohn, L. P. Kouwenhoven, and G. Schön (Kluwer, Dordrecht, 1997).

[2] S. M. Reimann and M. Manninen, Rev. Mod. Phys. **74**, 1283 (2002).

[3] G. Hackenbroich, Phys. Rep. **343**, 463 (2001).

[4] A. Yacoby, M. Heiblum, D. Mahalu, and H. Shtrikman, Phys. Rev. Lett. **74**, 4047 (1995).

[5] D. Loss and D. P. DiVincenzo, Phys. Rev. A **57**, 120 (1998).

[6] G. Burkard, D. Loss, and D. P. DiVincenzo, Phys. Rev. B **59**, 2070 (1999).

[7] I. Amlani, A. O. Orlov, G. Toth, G. H. Bernstein, C. S. Lent, and G. L. Snider, Science **284**, 289 (1999).

[8] E. Tekman and P. F. Bagwell, Phys. Rev. B **48**, 2553 (1993).

[9] X. R. Wang, Yupeng Wang, and Z. Z. Sun, Phys. Rev. B **65**, 193402 (2002).

[10] L. F. Santos and M. I. Dykman, Phys. Rev. B **68**, 214410 (2003).

[11] P. A. Orellana, F. Domínguez-Adame, I. Gómez, and M. L. Ladrón de Guevara, Phys. Rev. B **67**, 085321 (2003).

[12] K. Kobayashi, H. Aikawa, A. Sano, S. Katsumoto, and Y. Iye, Phys. Rev. B **70**, 035319 (2004).
[13] M. Sato, H. Aikawa, K. Kobayashi, S. Katsumoto, and Y. Iye, Phys. Rev. Lett. **95**, 066801 (2005).
[14] Y. Zheng, T. Lü, C. Zhang, and W. Su, Physica E (Amsterdam) **24**, 290 (2004).
[15] P. Stefański, A. Tagliacozzo, and B. R. Bułka, Phys. Rev. Lett. **93**, 186805 (2004).
[16] K. Bao and Y. Zheng, Phys. Rev. B **73**, 045306 (2005).
[17] A. A. Aligia and A. M. Lobos, J. Phys.: Condens. Matter **17**, S1095 (2005).
[18] M. E. Torio, K. Hallberg, S. Flach, A. E. Miroshnichenko, and M. Titov, Eur. Phys. J. B **37**, 399 (2004).
[19] Y. Liu, Y. Zheng, and T. Lü (unpublished).
[20] Y. Meir and N. S. Wingreen, Phys. Rev. Lett. **68**, 2512 (1992).
[21] A. P. Jauho, N. S. Wingreen, and Y. Meir, Phys. Rev. B **50**, 5528 (1994).
[22] Y. Meir, N. S. Wingreen, and P. A. Lee, Phys. Rev. Lett. **66**, 3048 (1991).
[23] S. Datta, *Electron Transport in Mesoscopic Systems* (Cambridge University Press, Cambridge, England, 1995).
[24] J. L. Li, J. F. Jia, X. J. Liang, X. Liu, J. Z. Wang, Q. K. Xue, Z. Q. Li, J. S. Tse, Z. Zhang, and S. B. Zhang, Phys. Rev. Lett. **88**, 066101 (2002).
[25] J. Jia, J. Z. Wang, Q. K. Xue, Z. Q. Li, Y. Kawazoe, and S. B. Zhang, Appl. Phys. Lett. **80**, 3186 (2002).
[26] M. W. Wu, J. Zhou, and Q. W. Shi, Appl. Phys. Lett. **85**, 1012 (2004).
[27] Q. W. Shi, J. Zhou, and M. W. Wu, Appl. Phys. Lett. **85**, 2547 (2004).
[28] G. Chen, G. Klimeck, S. Datta, G. Chen, and William A. Goddard III, Phys. Rev. B **50**, 8035 (1994).
[29] J. Q. You and H. Z. Zheng, Phys. Rev. B **60**, 13314 (1999).
[30] J. Q. You and H. Z. Zheng, Phys. Rev. B **60**, 8727 (1999).
[31] D. Goldhaber-Gordon, H. Shtrikman, D. Mahalu, D. Abusch-Magder, U. Meirav, and M. A. Kastner, Nature (London) **391**, 156 (1998).
[32] D. Goldhaber-Gordon, J. Gores, M. A. Kastner, H. Shtrikman, D. Mahalu, and U. Meirav, Phys. Rev. Lett. **81**, 5225 (1998).
[33] P. S. Deo and A. M. Jayannavar, Phys. Rev. B **50**, 11629 (1994).